Materials Science and Engineering A 528 (2010) 691–697

Contents lists available at ScienceDirect

Materials Science and Engineering A

journal homepage: www.elsevier.com/locate/msea

Titanium foams produced by solid-state replication of NaCl powders

Bing Ye, David C. Dunand*

Department of Materials Science and Engineering, Northwestern University, Evanston, IL 60208, USA

ARTICLE INFO

Article history:
Received 11 August 2010
Received in revised form
15 September 2010
Accepted 16 September 2010

Keywords:
Sodium chloride
Composites
Porous materials
Powder metallurgy
Low cost titanium

ABSTRACT

Open-celled titanium foams were fabricated by vacuum hot pressing of a blend of Ti and NaCl powders followed by NaCl removal in water. Densification kinetics of the Ti/NaCl blends are measured at 780 °C at various pressures (30–50 MPa), NaCl volume fractions (30–70%) and NaCl powder sizes (50–500 μm). As compared to pure Ti powders, densification kinetics of the blends is faster for relative densities below 92% due to rapid deformation of the NaCl powders. After dissolution, the flattened shape of the NaCl powders is replicated in the pores, resulting in an anisotropic porous structure. The foams exhibit good compressive strengths (e.g., 102 MPa for 50% porosity and 28 MPa for 67% porosity), low Young moduli (e.g., 29 GPa for 51% porosity) and ductile behavior up to compressive strain >60%.

1. Introduction

Titanium foams, inheriting attractive properties from titanium alloys, show high specific strength, stiffness and energy absorption together with excellent corrosion resistance and biocompatibility, making them applicable in fields ranging from biomaterial [1–3] to transportation [4,5]. Titanium foams are particularly interesting for bone implants because of their low stiffness (which reduces the stress shielding effect due to the stiffness mismatch between implant and bone [1,6]) and because bone growth can occur within the porosity, if a minimum diameter of ~100 μm [1,7,8] is achieved, thus improving anchorage of the implant [9].

Due to the high melting point, strong reactivity and acute contamination tendency of liquid titanium, various solid-state processes based on titanium powder densification have been developed to create titanium foams, as reviewed in Refs. [4,10]. Expansion of trapped gas [11–13], partial sintering of powders [14,15], or electron beam/laser melting of powders [16–18] are existing methods where porosity is created in titanium without space-holders. The use of space-holders allows for simple and accurate control of pore fraction, shape and connectivity in titanium, and the focus to date has been on temporary, fugitive space-holders (e.g., magnesium [19], sodium chloride [20], polymers [21,22], camphene [23], ammonium hydrogen carbonate [24] and ice [25]) which evaporate or decompose during the temperature ramp leading to the final sintering temperature. However, microporosity within the Ti struts is often present, as a result of incomplete sintering. By contrast, a space-holder remaining during the entire titanium powder densification process allows the use of pressure to enhance the densification of the titanium powders. Recently, steel has been used as permanent space-holder in Ti and Ti–6Al–4V, with the removal from the densified composites occurring by electrochemical means [26,27]. This second step in the process can be slow, so it is desirable to use as space-holder a salt which is chemically inert with titanium at the high temperature used during the densification step, but can be removed rapidly at ambient temperature by simple immersion in water. This approach was demonstrated for NiTi foams which used as space-holders acid-soluble NaF [28,29] or water-soluble NaCl [30] powders. NaCl was however molten at the temperatures needed to densify the NiTi powders, thus requiring encapsulation of the metal/salt powder blend in a steel container [30].

In the present article, we demonstrate the creation of titanium foams using solid NaCl space-holders by hot pressing at 780 °C at various pressures (30–50 MPa), NaCl volume fractions (30–70%) and NaCl sizes (50–500 μm). We measure densification kinetics of Ti/NaCl blends as a function of these variables, and report on the structure and mechanical properties of the resulting foams after NaCl dissolution.

2. Experimental procedures

2.1. Materials

The titanium powders used were angular HDH (hydrogenation/de-hydrogenation) titanium of commercial purity, shown in Fig. 1a,

* Corresponding author at: Department of Materials Science and Engineering, Northwestern University, 2225 North Campus Drive, Evanston, IL 60208, USA.
Tel.: +1 847 491 5370; fax: +1 847 467 6573.
E-mail address: dunand@northwestern.edu (D.C. Dunand).

0921-5093/$ – see front matter © 2010 Elsevier B.V. All rights reserved.
doi:10.1016/j.msea.2010.09.054

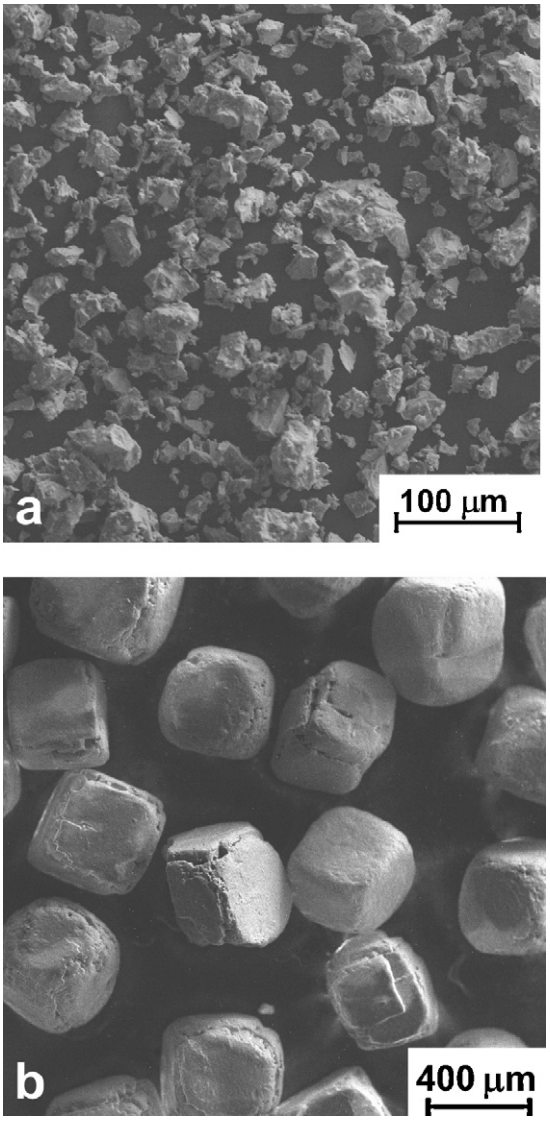

Fig. 1. SEM micrographs of (a) 30–44 μm angular titanium powders; (b) 355–500 μm sodium chloride powders with cuboidal shape.

supplied by Phelly Materials (Bergenfield, NJ), sieved to −325 mesh (30–44 μm) and with oxygen content of 0.42 wt% (ASTM grade 4). The microhardness of mounted and polished powder was 217 ± 13 HV, corresponding to a yield strength of 602 ± 13 MPa (using a conversion factor of 3.6 [31,32]), within the range of 480–635 MPa for commercial-purity Ti ASTM grade 4 [33]. The cuboidal sodium chloride powders (∼99% pure, iodide-free, NaCl from Morton Salt) shown in Fig. 1b were sieved to different size ranges: 50–100, 100–200, 355–500, and 100–500 μm.

A few control experiments were carried out with angular HDH Ti–6Al–4V powders with a typical size of 100 × 200 μm and the following composition (in wt.%): 5.50–6.75% Al, 3.50–4.50% V, 0.30% Fe, 0.20% O, 0.08% C, 0.05% N and 0.015% H (ASTM F 1580-1).

2.2. Ti/NaCl blend densification

Blends of Ti and NaCl powders were thoroughly mixed by tumbling for 20 min in a polypropylene round-bottom bottle with a single central baffle [34]. All blends were hot pressed in cylindrical dies at 780 °C under a vacuum of 5×10^{-5} torr (further experimental details concerning the uniaxial hot pressing procedures are reported in Ref. [35]). Small samples used for pore morphology and ultrasonic experiments were densified from blends with 350–500 μm NaCl powders at 40 MPa for 2 h in a graphite die (6.6 mm ID, 63.5 mm OD and 34.3 mm height), using tungsten pistons. Large samples for densification study were pressed until densification rates became negligible in a cylindrical TZM molybdenum die (25.4 mm ID, 63.5 mm OD and 34.3 mm height) using TZM pistons. NaCl fractions and size distributions in the blends as well as applied stresses were varied for these samples, which were also used for mechanical property measurements.

The density of the large Ti/NaCl samples, with a height of ∼12 mm, was measured by the Archimedes method in ethanol (denatured, 95 vol.%, EMD Chemicals, Inc., Gibbstown, NJ). Ethanol, with a density of 0.809 g/cm^3 at room temperature (supplier information), was chosen because it dissolves neither NaCl nor vacuum grease. Using the measured final density and the piston displacement data, the Ti/NaCl sample relative density (with an error about 0.3%) was then calculated during the densification experiment, as previously described in Ref. [35].

2.3. Ti foams

After density measurement of the Ti/NaCl composites, the NaCl phase was dissolved in deionized water to obtain Ti foams. Complete removal of the NaCl was observed after 2–3 h for samples with ∼1.5 g mass, and foam metal density measured by helium pycnometer was equal to the theoretical density of titanium (4.51 g/cm^3), indicating that no closed porosity was present. Oxygen and sodium content of the foams, as measured by chemical analysis (performed by Luvak, Inc., Boylston, MA) were 0.48% and 0.052 wt.%, respectively. Thus, the oxygen contamination due to hot pressing was small (0.06%) and the NaCl space-holder removal was near complete.

Metallographic sample preparation for the small foam samples for scanning electron microscope (SEM) imaging followed Ref. [35] and consisted of 9 μm and 1 μm diamond suspension polishing and 0.05 μm colloidal silica final polishing. The Young's modulus in the direction of the densification stress was measured ultrasonically, using 2.25 MHz and 5 MHz ultrasonic transducers in transmission mode, on cylindrical samples with 5.1 mm diameter and 7.8 mm height. Cylindrical foam samples with 5 mm diameter and 11 mm height were cut by electro-discharge machining with their height parallel to the height of the larger densified billet. They were tested in compression on a MTS Sintech 20/G tensile tester at a strain rate of 5×10^{-4} s^{-1} to a final strain of ∼60%, using a compression cage to insure parallelism, with strain determined by cross-head displacement after calibration with aluminum sample and taking into account compliance of the load train. An extensometer was attached to the compression sample for direct strain measurement during the first 1% strain.

3. Results and discussion

3.1. Choice of space-holder

We selected here NaCl as a permanent space-holder because of its high solubility in water (359 g/L at room temperature), complete inertness with titanium, and very low toxicity (important if small quantities of space-holder remain in the foams used as biomedical implants). However, unlike the previous research where NiTi powders were densified by hot isostatic pressing (HIP) at temperatures where the NaCl phase was liquid [20,30], we use here a temperature below the melting point of NaCl (801 °C). This is possible because Ti is much less creep resistant than NiTi [36,37], so that titanium powders can be densified at lower temperatures than NiTi powders at a given stress and for a given time. Avoiding liquid NaCl then allows powder densification to occur in a die by uniaxial hot-pressing,

rather than in a closed canister used in HIP densification. In turn, this permits the use of shaped dies capable or creating near-net-shape objects, unlike HIP densification of billets within canisters; furthermore, as compared to HIP, it eliminates the steps of sealing and removing the steel canister before and after densification.

The Hunter process creates a mixture of Ti and NaCl powders by reduction of $TiCl_4$ with liquid sodium, and the salt is removed by washing in water to create pure Ti powders [33]. This latter step increases the cost of the powders and also potentially increases their oxide content. The present method could use Ti–NaCl mixtures (with Ti/NaCl volume ratio of ~0.1) as-synthesized by the Hunter process and without washing to create directly titanium foams. It would be however necessary to reduce the NaCl fraction (and thus the pore fraction) to below 80%, so the titanium phases become percolating after densification. This could be achieved by additions of pure Ti powders or partial removal of NaCl through partial washing.

3.2. Microstructure of Ti foams

SEM images of cross-sections of foams with 50 and 60% porosities are shown in Fig. 2 in radial cross-sections and in Fig. 3 in longitudinal cross-sections. These figures confirm that near-complete densification of the titanium matrix is achieved, with small amounts of fine (<10 μm) porosity visible only in a few places (arrows in Fig. 2). Thin Ti struts between pores (Fig. 2b and d) illustrate that even small volumes of titanium powders can be well densified under the present conditions (780 °C/40 MPa/2 h).

In radial sections (Fig. 2), the primary pores, which are uniformly distributed, replicate the size and shape of the angular NaCl particles with rounded corners. Thus, pore shape can be controlled by using NaCl powders with various shapes which can be controlled, e.g., by anti-solvent crystallization [38]. In the longitudinal sections (Fig. 3), the primary pores are flattened, with the small pore dimension parallle to the hot-press loading direction, indicating that the NaCl powders deformed in the direction of the stress applied by the pistons. The creep deformation of the NaCl powders occurred most probably during the early stages of densification, when pressure was not yet fully isostatic in the die, as the Ti powders were only lightly connected. Deformation occurred because NaCl has a much lower creep strength than Ti [39]: at 780 °C, the shear strain rate of NaCl is higher than that of Ti by factors $>3 \times 10^5$ for 1–10 MPa shear stress and >20 for 100 MPa shear stress. Only once the NaCl powders are in near hydrostatic state within a packed bed of Ti powders and do not deform, densification between Ti powders becomes the dominant densification mechanism.

Anisotropic pore shape allows control of mechanical and physical properties (e.g., stiffness, strength and permeability) and is thus desirable in some applications. For instance, elongated pores in titanium bone implants can mimic the structure of bone which accounts for its mechanical anisotropic properties. Elongated pores have recently been created in titanium by swaging of Ti/camphene powder blends, followed by evaporation of the deformed camphene space-holders and sintering of the Ti powders at 1070 °C [40]. However, carbon contamination and incomplete Ti sintering were reported. The use of NaCl as an inert, permanent space-holder addresses these issues, and hot extrusion of NaCl/Ti blends at 780 °C may provide complete densification of Ti powders (due to the high deviatoric stresses present during extrusion) as well as elongation of the NaCl space-holders (from the high plasticity of NaCl at elevated temperature).

The inner surface of the primary pores is rough, with the shape and size of the original Ti powders visible (Figs. 2 and 3). This indicates that the Ti powders indented the weaker NaCl powders during hot pressing, and that surface diffusion at 780 °C was not sufficient to smooth the pores, as expected given the very high melting

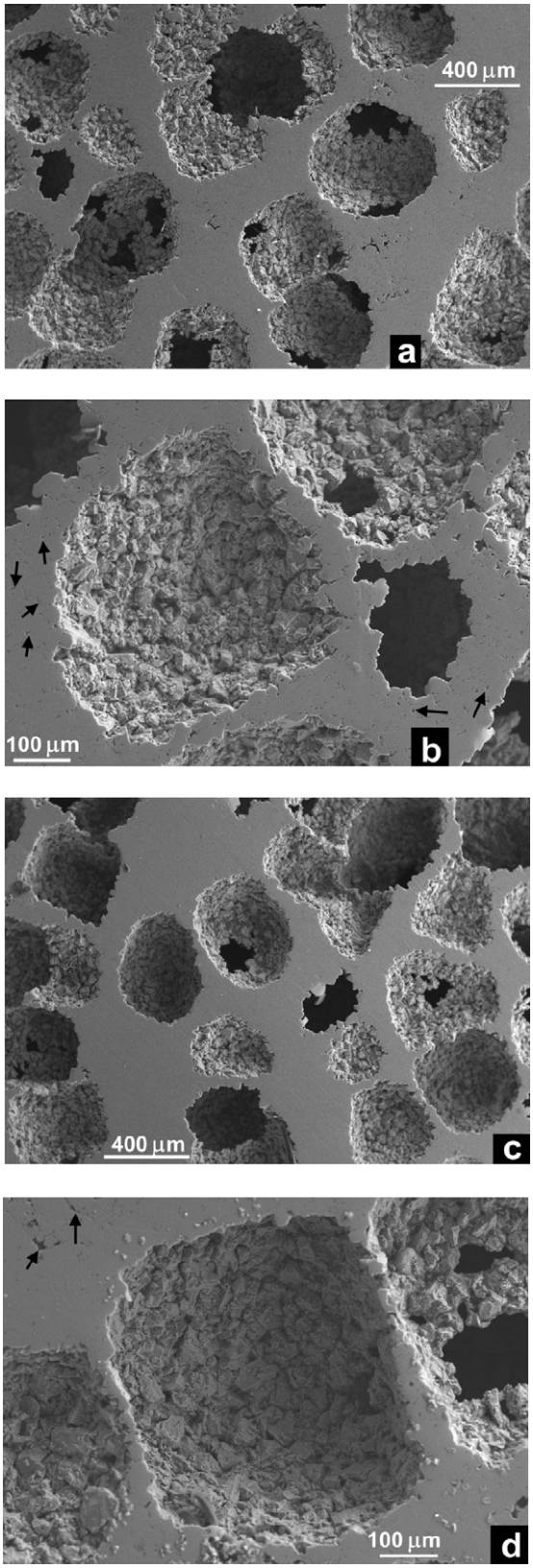

Fig. 2. SEM micrographs of radial cross-sections of titanium foams created with 355–500 μm NaCl powders showing (a, b) 50 vol.% porosities at low and high magnification, (c, d) 60 vol.% porosities at low and high magnification. Hot press loading was perpendicular to sections.

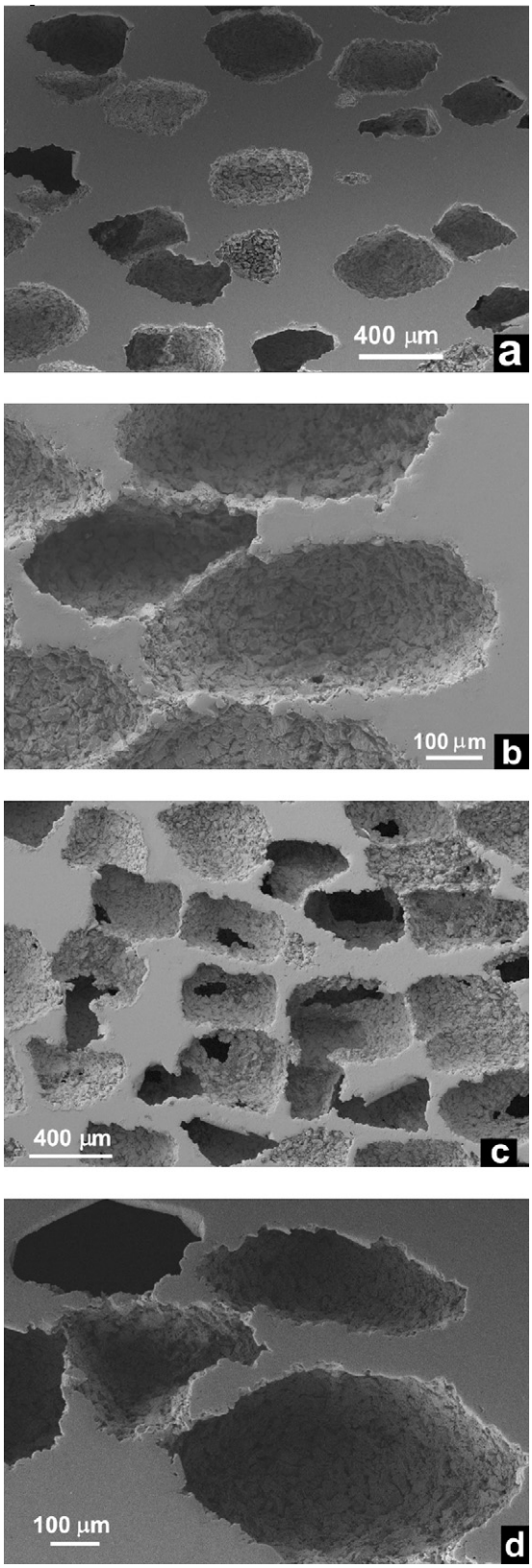

Fig. 3. SEM micrographs of longitudinal cross-sections of titanium foams created with 355–500 μm NaCl powders showing (a, b) 50 vol.% porosities at low and high magnification, (c, d) 60 vol.% porosities at low and high magnification. Hot press loading was vertical.

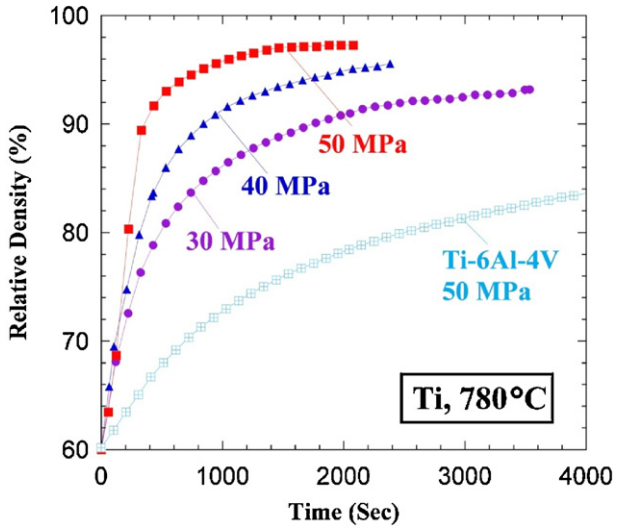

Fig. 4. Densification curves for pure Ti powders under 30, 40 and 50 MPa stress at 780 °C. A curve for Ti–6Al–4V powders under 50 MPa stress is also shown.

point of titanium (1668 °C). Surface roughness has been shown to enhance bone growth [41] and the roughness of the inner pore surfaces in the present Ti foams can be modified by heat-treatment or acid dissolution. Finally, in Figs. 2 and 3, fenestrations between pores are visible either as black pores (due to the limited depth of field of the SEM) or as necks between adjacent pores in cross-sections. These fenestrations often exceed 100 μm in diameter, the critical size for bone ingrowth [1,7,8], indicating that bone may be able to penetrate deep into the porous structure.

3.3. Densification kinetics of Ti/NaCl blends

Densification curves plotted as relative density vs. time for Ti powders without NaCl are shown in Fig. 4 for applied stresses of 30, 40 and 50 MPa. The densification rate decreases with time and increases with applied stress, as also reported by Taylor et al. [42] for pure Ti powders hot-pressed at similar temperature and pressures. Further comparisons with this work are not made, because of the much slower densification (e.g., at 800 °C and 50 MPa, the relative density was ~82% after 3000 s [42]) due to the use of a smaller die leading to significant friction, as quantified in Ref. [43]. Fig. 4 shows that, at 50 MPa, the Ti powders reach 97% relative density within 40 min. For comparison, Ti–6Al–4V attains 79% relative density at the same pressure and times, indicating that significantly higher stresses (maybe in the typical range of HIP presses and hot extrusion machines) are needed to achieve full densification, given that the densification temperature must remain below the 801 °C melting point of NaCl.

The densification curves of Ti–50% NaCl blends for 30, 40 and 50 MPa applied stresses (Fig. 5) display, as expected, the same trends as for pure Ti (Fig. 4): densification rates decrease with time and increase with applied stress. Fig. 6 compares densification curves for Ti (Fig. 4) and for Ti–50 vol.% NaCl (Fig. 5), with curves shifted along the time axis so they all initiate at the same density of 65%. Two trends are visible in Fig. 6. First, the presence of NaCl accelerates densification for relative densities below ~94%; second, the final density, extrapolated with dotted lines in Fig. 6 for long times, is nearly unaffected by the presence of NaCl. Because the low stress curves are below the 94% density range for the present experiment times of ~3000 s, the first effect (NaCl enhancement of densification) is most visible for 30 MPa, less apparent for 40 MPa and least visible for 50 MPa (in fact, for this stress, the pure Ti experiment shows slightly higher densities at all densification times). Simi-

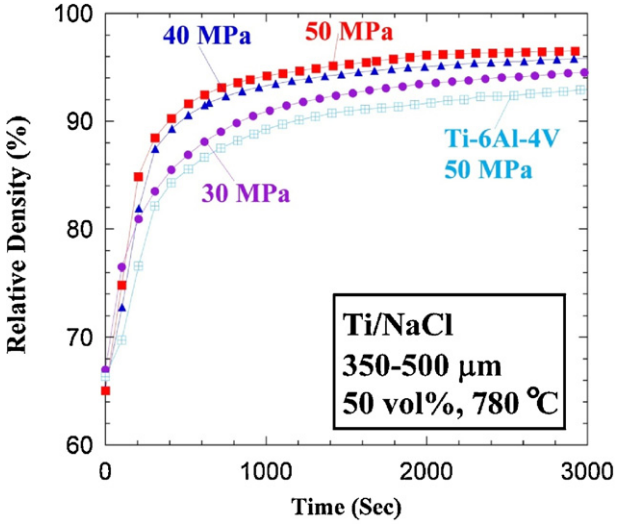

Fig. 5. Densification curves for blends of Ti/50 vol.% NaCl (355–500 μm) powders under 30, 40 and 50 MPa stress at 780 °C. A curve for Ti–6Al–4V/50 vol.% NaCl (355–500 μm) under 50 MPa is also shown.

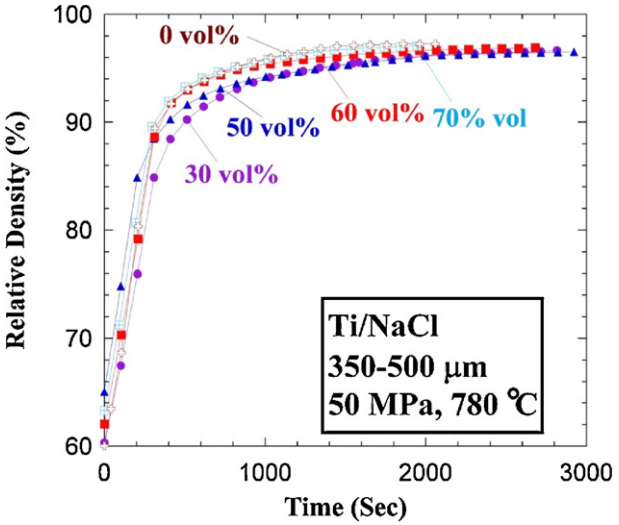

Fig. 7. Densification curves for Ti/NaCl (355–500 μm) powder blends under 50–MPa stress at 780 °C for NaCl volume fractions of 0, 30, 50, 60 and 70%.

larly, densification of Ti–6Al–4V/50 vol.% NaCl at 50 MPa (Fig. 5) is much faster than for pure Ti–6Al–4V powder (Fig. 4), with the curves remaining below 94% density at all times.

These observations can be well explained by the previously discussed mechanisms of densification of Ti/NaCl blends: at first, weak NaCl powders deform rapidly, explaining the initial enhancement of densification rates. Then, densification occurs among the stronger Ti powders, justifying that the final density is unaffected by NaCl. This scenario is consistent with, but opposite to, that put forward for previous densification experiments conducted at similar temperatures and pressures (870 °C and 25–50 MPa) for Ti/10 vol.% TiC powder blends: the composite blends showed densification rate lower by a factor 5 than pure Ti, for a given stress and density [42]. In that case, the TiC powders are non-deforming, so load is transferred to them from the creeping, densifying Ti matrix, thus reducing the stress on the Ti powders that drives densification. Furthermore, the shrinkage rate is reduced for pairs of TiC and Ti powders (which had a similar size, unlike the present Ti/NaCl powders), since only the latter deform. Finally, the initial packing densities of the blends was lower than pure Ti for the Ti/10 vol.% TiC powder blends [42] but higher for the present Ti/NaCl blends. This increased packing density is due to the large difference in powder sizes between Ti and NaCl (Fig. 1).

Densification curves for blends with 30, 50, 60 and 70 vol.% NaCl (all with 355–500 μm size) are shown in Fig. 7. Differences among these various Ti/NaCl blends are very small, confirming that, at 50 MPa, NaCl powders do not control the densification kinetics. This is likely to hold true up to near the point where Ti powders become non-percolating in the blend, i.e., ~17 vol.% for spherical particles [44] (corresponding to ~83 vol.% NaCl). Above the percolation limit, the Ti powders form a continuous network within the blend, and the densification between pairs or clusters of Ti powders becomes controlling.

Finally, Fig. 8 shows that the NaCl powder size has no significant effect on densification kinetics for a constant volume fraction of 50% at a stress of 50 MPa. This is in agreement with theoretical powder densification models [45,46] that are insensitive to powder size, and it is consistent with the above mechanism where final density is dictated by the densification of the Ti powders rather than NaCl powders.

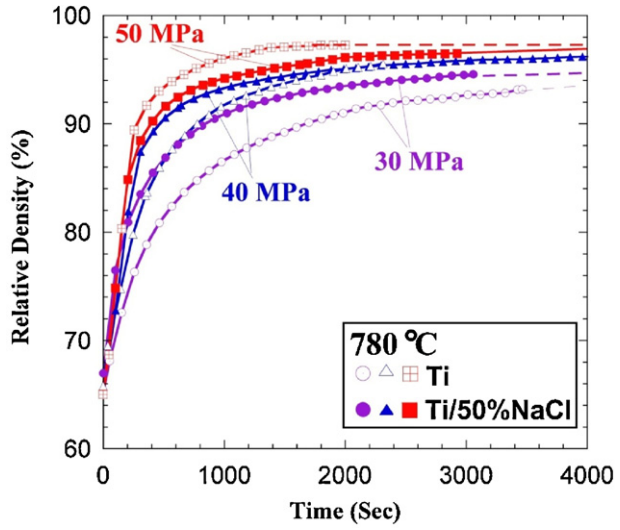

Fig. 6. Densification curves for Ti and blends of Ti/50 vol.% NaCl (355–500 μm) powders under 30, 40 and 50 MPa stress at 780 °C.

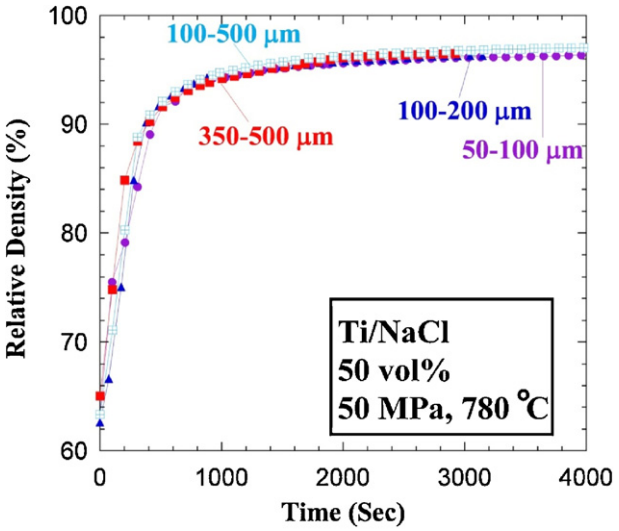

Fig. 8. Densification curves for Ti/50 vol.% NaCl (355–500 μm) powder blends under 50 MPa stress at 780 °C for NaCl size ranges of 50–100, 100–200, 355–500, and 100–500 μm.

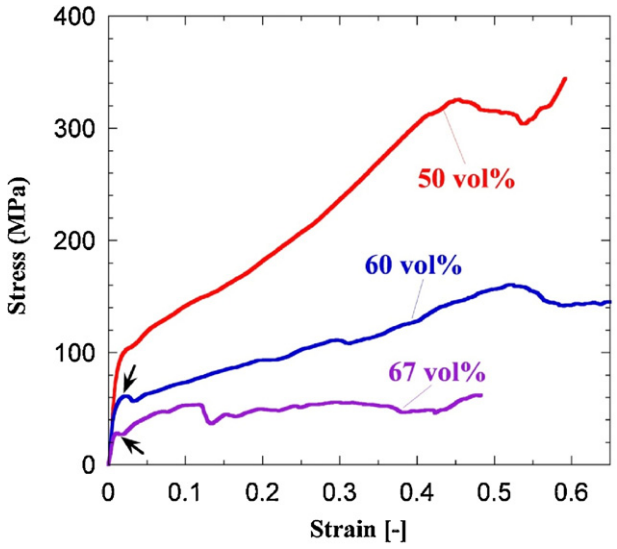

Fig. 9. Compressive stress–strain curves for Ti foams with 50, 60, and 67% porosity.

3.4. Mechanical properties of Ti foams

Ultrasonic measurement of foams with 42 and 51% porosity provide Young's modulus values of 39 GPa and 29 GPa, respectively. These values are in reasonable agreement with moduli of 35 and 25 GPa predicted from the Gibson–Ashby model for open-cell foams [47]:

$$E^* = E_s \cdot \left(\frac{\rho^*}{\rho_s}\right)^2 \quad (1)$$

where E^* and E_s are Young's moduli of foam and bulk materials with densities ρ^* and ρ_s, respectively, using E_s = 105 GPa for Ti [33]. This model does not take into account the non-equiaxed shape of the porosity.

Compressive stress–strain curves are shown in Fig. 9 for foams with 50, 60, and 67% pores (as measured on the machined specimens). Measured stiffnesses from stress–strain curves are 11, 8, and 4 GPa, respectively, calculated after load-frame compliance correction. Stiffness values from direct extensometry measurements are 13, 8 and 14 GPa. Both sets of values are lower than the Gibson–Ashby model (Eq. (1)) predictions which are 26 and 16 and 11 GPa. This may reflect experimental difficulties associated with accurate displacement measurements for small, compliant samples, but is also probably linked with the onset of localized plasticity and damage in the linear portion of the stress–strain curve, produced by stress concentrations within the foam and exacerbated by the non-spherical shape of the pores.

Foams with 50, 60, and 67% porosity exhibit yield stresses of 102, 61 and 28 MPa, respectively (Fig. 9). These yield stresses are somewhat higher than those reported by Esen and Bor [19] (89, 40 and 18 MPa for 53, 62, and 70% porosity, respectively) for titanium foams created with magnesium space-holders by room temperature cold pressing at 500 MPa followed by sintering at 1200 °C. The higher strength of the present foam may originate from the fuller densification of the titanium struts achieved under hot pressing as compared to pressureless vacuum sintering [19].

Finally, Fig. 9 demonstrates that the titanium foams exhibit ductile-like behavior up to compressive strains of 50% or above, well beyond the range useful for bone implants but over the range where extensive energy absorption occurs by collapse of pores. The post-yield stress drops recorded in foams with 60 and 67% porosity (marked with arrows in Fig. 9) correspond to macroscopic shearing of the sample which may be exacerbated by the notch effect from the elongated pores oriented with their main axes perpendicular to the applied stress.

4. Conclusions

Titanium foams with porosities of 30–70% have been produced by hot pressing of Ti/NaCl powder blends at 780 °C followed by dissolution of NaCl. The following main conclusions are reached:

1. NaCl is an attractive permanent space-holder for Ti powder densification for various reasons: (i) the high melting point of NaCl (as compared to previous fugitive space-holders used with Ti) allows full densification of Ti/NaCl blends at high pressures and temperature, ensuring the elimination of microporosity between Ti powders; (ii) NaCl is chemically unreactive with Ti, thus preventing contamination and degradation of mechanical properties; (iii) NaCl is highly soluble in water and can therefore be rapidly removed to create porosity; (iv) NaCl is non toxic and inexpensive.
2. For densification times <1 h and relatively low stresses of 30–50 MPa, the titanium powders are nearly completely densified, insuring that the foam, after removal of the NaCl space-holder, has good mechanical properties. A foam with 50% porosity exhibits a Young's modulus of 29 GPa, a compressive yield stress of 102 MPa, and ductile-like behavior for compressive strains >50%. Strength and stiffness decrease as porosity increases.
3. At the 780 °C hot pressing temperature, the NaCl powders deform much faster than the titanium powders. This results in faster densification of the Ti/NaCl blends as compared to pure Ti, and in flattening of the NaCl powders perpendicular to applied stress. The replicated pores created in the foam by NaCl removal therefore show elongated shapes that may be useful if foams with anisotropic structure and properties are desired.

Acknowledgements

This research was supported by the Initiative for Sustainability and Energy at Northwestern. The authors thank Mr. Andrew Ball (Northwestern University) for preliminary feasibility experiments and for assistance with preparing samples shown in Fig. 2 and used for ultrasonic measurements. They also acknowledge Mr. Anselm Neurohr (Northwestern U.) for assistance with compression testing on Ti-foams and Ms. Peiqi Zheng (Northwestern U.) for assistance with SEM imaging for Fig. 3a and d.

References

[1] M. Geetha, A.K. Singh, R. Asokamani, A.K. Gogia, Progress in Materials Science 54 (2009) 397–425.
[2] X. Wang, Y. Li, J. Xiong, P.D. Hodgson, C.E. Wen, Acta Biomaterialia 5 (2009) 3616–3624.
[3] G. Ryan, A. Pandit, D.P. Apatsidis, Biomaterials 27 (2006) 2651–2670.
[4] J. Banhart, Progress in Materials Science 46 (2001) 559–632.
[5] L.-P. Lefebvre, J. Banhart, D.C. Dunand, Advanced Engineering Materials 10 (2008) 775–787.
[6] E.D. Spoerke, N.G.D. Murray, H. Li, L.C. Brinson, D.C. Dunand, S.I. Stupp, Journal of Biomedical Materials Research Part A 84A (2008) 402–412.
[7] V. Karageorgiou, D. Kaplan, Biomaterials 26 (2005) 5474–5491.
[8] W. Xue, B.V. Krishna, A. Bandyopadhyay, S. Bose, Acta Biomaterialia 3 (2007) 1007–1018.
[9] E.D. Spoerke, N.G. Murray, H. Li, L.C. Brinson, D.C. Dunand, S.I. Stupp, Acta Biomaterialia 1 (2005) 523–533.
[10] D.C. Dunand, Advanced Engineering Materials 6 (2004) 369–376.
[11] N.G.D. Murray, D.C. Dunand, Composites Science and Technology 63 (2003) 2311–2316.
[12] N.G.D. Murray, D.C. Dunand, Acta Materialia 52 (2004) 2269–2278.
[13] I.M. Robertson, G.B. Schaffer, Powder Metallurgy 53 (2010) 27–33.
[14] Y. Sakamoto, K. Asaoka, M. Kon, T. Matsubara, K. Yoshida, Bio-medical Materials & Engineering 16 (2006) 83–91.
[15] P.A. Noel, D.C. Dunand, A. Mortensen, Composites 25 (1994) 953–956.

[16] L.E. Murr, S.M. Gaytan, F. Medina, E. Martinez, J.L. Martinez, D.H. Hernandez, B.I. Machado, D.A. Ramirez, R.B. Wicker, Materials Science and Engineering A 527 (2010) 1861–1868.
[17] P. Heinl, A. Rottmair, C. Korner, R.F. Singer, Advanced Engineering Materials 9 (2007) 360–364.
[18] V.K. Balla, S. Bose, A. Bandyopadhyay, Philosophical Magazine 90 (2010) 3081–3094.
[19] Z. Esen, S. Bor, Scripta Materialia 56 (2007) 341–344.
[20] Y. Orlova, K. Maekawal, H.J. Rack, in: M. Cabibbo, S. Spigarelli (Eds.), Recent Developments in the Processing and Applications of Structural Metals and Alloys, Trans Tech Publications Ltd., Stafa-Zurich, 2009, pp. 411–417.
[21] C. Jee, Z. Guo, J. Evans, N. Ozguven, Metallurgical and Materials Transactions B 31 (2000) 1345–1352.
[22] A. Manonukul, N. Muenya, F. Leaux, S. Amaranan, Journal of Materials Processing Technology 210 (2010) 529–535.
[23] M. Bram, C. Stiller, H.P. Buchkremer, D. Stover, H. Baur, Advanced Engineering Materials 2 (2000) 196–199.
[24] C.E. Wen, Y. Yamada, K. Shimojima, Y. Chino, H. Hosokawa, M. Mabuchi, Journal of Materials Research 17 (2002) 2633–2639.
[25] Y. Chino, D.C. Dunand, Acta Materialia 56 (2008) 105–113.
[26] P.J. Kwok, S.M. Oppenheimer, D.C. Dunand, Advanced Engineering Materials 10 (2008) 820–825.
[27] D.J. Jorgensen, D.C. Dunand, Materials Science and Engineering A 527 (2010) 849–853.
[28] A. Bansiddhi, D.C. Dunand, Intermetallics 15 (2007) 1612–1622.
[29] A. Bansiddhi, T.D. Sargeant, S.I. Stupp, D.C. Dunand, Acta Biomaterialia 4 (2008) 773–782.
[30] A. Bansiddhi, D.C. Dunand, Acta Biomaterialia 4 (2008) 1996–2007.
[31] H. Conrad, Progress in Materials Science 26 (1981) 123–403.
[32] Atlas of Stress–Strain Curves, 2nd ed., ASM International, Materials Park, OH, 2002.
[33] G. Lutjering, J.C. Williams, Titanium, 2nd ed., Springer-Verlag, New York, 2007.
[34] J.M. Ottino, R.M. Lueptow, Science 319 (2008) 912–913.
[35] B. Ye, M.R. Matsen, D.C. Dunand, Acta Materialia 58 (2010) 3851–3859.
[36] C. Schuh, D.C. Dunand, Scripta Materialia 45 (2001) 1415–1421.
[37] S.M. Oppenheimer, A.R. Yung, D.C. Dunand, Scripta Materialia 57 (2007) 377–380.
[38] C. Gaillard, J.F. Despois, A. Mortensen, Materials Science and Engineering A 374 (2004) 250–262.
[39] H.J. Frost, M.F. Ashby, Deformation-Mechanism Maps: The Plasticity and Creep of Metals and Ceramics, 1st ed., Pergamon Press, 1982.
[40] Y. Chino, D.C. Dunand, Advanced Engineering Materials 11 (2009) 52–55.
[41] H. Daugaard, B. Elmengaard, J.E. Bechtold, K. Soballe, Journal of Biomedical Materials Research Part A 87A (2008) 434–440.
[42] N. Taylor, D.C. Dunand, A. Mortensen, Acta Metallurgica et Materialia 41 (1993) 955–965.
[43] B. Ye, M.R. Matsen, D.C. Dunand, in preparation.
[44] F.F. Lange, L. Atteraas, F. Zok, J.R. Porter, Acta Metallurgica et Materialia 39 (1991) 209–219.
[45] E. Arzt, M. Ashby, K. Easterling, Metallurgical and Materials Transactions A 14 (1983) 211–221.
[46] C. Schuh, P. Noel, D.C. Dunand, Acta Materialia 48 (2000) 1639–1653.
[47] L.J. Gibson, M.F. Ashby, Cellular Solids: Structure and Properties, 2nd ed., Cambridge University Press, 1999.